

RAL 95038

COPY 2 R61 RR

ACCN: 226165

DRAL

Daresbury Laboratory
Rutherford Appleton Laboratory

RAL Report

RAL-95-038

Rate and Lifetime Characteristics of a Gas Microstrip Detector Fabricated on Thin D263 Glass

J E Bateman et al

April 1995

Rutherford Appleton Laboratory Chilton DIDCOT Oxfordshire OX11 0QX

**DRAL is part of the Engineering and Physical
Sciences Research Council**

The Engineering and Physical Sciences Research Council
does not accept any responsibility for loss or damage arising
from the use of information contained in any of its reports or
in any communication about its tests or investigations

**RATE AND LIFETIME CHARACTERISTICS OF A GAS MICROSTRIP DETECTOR
FABRICATED ON THIN D263 GLASS**

**J E Bateman and J F Connolly,
Rutherford Appleton Laboratory, Chilton, Didcot, OX11 0QX, UK**

**R Mutikainen and I Suni,
VTT Electronics, Otakaari 7 B, FIN-02150 Espoo, Finland**

The rate and aging characteristics of a gas microstrip detector fabricated on thin ($200\mu\text{m}$) borosilicate glass (D263) are reported. The use of a high drift field (7kV/cm) and a back electrode at the same potential as the anode led to promising rate and short-term aging characteristics. In the longer term, however, the effects of ion movement in the substrate have been found to be very deleterious.

1. INTRODUCTION

Following the introduction of the gas microstrip detector (GMSD) by Oed [1], we have studied a wide range of substrate and processing options for the construction of detectors which could show the rate and lifetime properties required by the demanding conditions likely to be met in LHC tracker facilities [2,3,4,5]. In our early work we found that semi-insulating substrate materials which depended on ionic conduction mechanisms (such as borosilicate glasses) are unstable in respect of rate and lifetime performance. On the other hand, we found that the use of an electronic semiconducting glass (such as Schott S8900) as the substrate produced unconditionally stable detectors which, with attention to the processing methods and to the gas system offer the prospect of a useful lifetime long enough for the hostile conditions of LHC. The principal drawback of S8900 glass is the high mean atomic number of the constituents which leads to a radiation length almost half that of a borosilicate glass. It is also a mechanically poor material so that handling sheets of thickness around $100\mu\text{m}$ (necessary to keep the scattering to an acceptable level) is foreseen to be a serious problem. We were interested, therefore, to see reported the successful high rate operation of a GMSD fabricated on a borosilicate glass (Desag D263) [6,7]. The thin substrate was operated with a back electrode at the anode potential and the drift field was moderately high ($\approx 5\text{kV/cm}$). In these conditions rate capability up to $\approx 10^6$ events/ mm^2/s was observed. The gain remained unaffected out to an accumulated charge of 40mC/cm but when irradiated at lower rates aging appeared to occur [7].

In order to check these important findings we constructed a GMSD using a $200\mu\text{m}$ thick D263 substrate coated with a Ni/Au metallisation and investigated its rate and lifetime properties when operated under the conditions described above.

2. EXPERIMENTAL SET-UP

The detector plate was fabricated using our standard test mask. The anode width is $10\mu\text{m}$, the cathode width $90\mu\text{m}$ and the anode cathode gap is $100\mu\text{m}$. Twenty anodes (and cathodes) of 60mm active length are bussed together giving a 6mm active width. The pattern is repeated five times on a plate of overall dimensions $100\text{mm} \times 100\text{mm}$. The metallisation (performed at VTT Electronics) is a 100nm -thick nickel film coated with electroplated gold to an overall thickness of $0.6\mu\text{m}$. On the reverse side of the plate a coating of chromium was sputtered.

The lithographic plate was supported on structures of standard glass-epoxy circuit boards housed in an aluminium box with a rubber seal and an aluminised melinex window ($50\mu\text{m}$) for xray access. Electrical leadthroughs are standard SHV connectors sealed with epoxy. In order to achieve high drift fields the drift electrode was spaced at 5mm from the lithographic plate.

A gas mixture of argon with 29%DME was supplied by our "clean" gas mixing system as described in reference [5].

We used the electronics readout system described in reference [5] and the same calibration procedures for the gain and the rate. The same xray test beam was used which can deliver $> 10^6$ 8keV xray events into a spot 1mm diameter.

The bias conditions for all tests were as follows: Drift potential = -3.5kV (i.e. 7kV/cm), Cathode potential = -626V and Anode potential (=Back plane potential) = 0V.

3. RESULTS

On applying the cathode bias the usual effect of substrate ion movement was observed in the 20% gain decrease observed to take place over a period of approximately one hour (figure 1). Once settled the detector showed excellent uniformity (figure 2) and a very good pulse height resolution (12% fwhm). It was observed that the cathode potential required to achieve a gain of 800 is considerably higher (by about 80V) than that normally required by this pattern. This is no doubt due to the effect of the back electrode at anode potential. It was also noted that any attempt to achieve a gain greater than 1000 resulted in sparking.

Figure 3 shows that the drift field in the counter contributes substantially to the gain process and that the full value of the drift field (7kV/cm) is required to overcome the recombination losses in the high concentration of DME and achieve the optimum pulse height resolution of 12%.

Figure 4 shows the behaviour of the counter gain when the xray beam intensity is steadily increased and the pulse height of the 8keV xrays is read off the CRT screen (this process occupying a few minutes only). This rate capability (no shift to 200kHz/mm² and only a 15% deficit at 525kHz/mm²) is very impressive compared to the poor performance which we observed on thick borosilicate substrates [2]. When one studies the rate performance systematically by applying a given rate to a fresh area of plate and following the gain in time, one again finds the complex effects which we observed previously in borosilicate substrates [2]. Figure 5 shows the results of applying this procedure with varying rates. The behaviour of the gain shows two stages: an initial dip followed by a rise. The length of the initial dip (of about 5%) is dose dependent indicating that a fixed amount of charge is moving (5 minutes at 1kHz/mm² and 1.5 minutes at 3kHz/mm²) and the dip is followed by a steady rise which is dose-dependent in magnitude and appears to have a time constant similar to that of the initial settling curve. When one plots the asymptotic gain for each rate measurement the result (figure 6) shows an approximately linear dependence on the logarithm of the count rate density. It is clear from figure 5 that with this detector one could experience rate-dependent gain shifts of up to $\approx 10\%$ in an LHC environment with intrinsic time constants of around one hour.

For lifetime testing the xray beam was applied to a constant spot in the middle of a detector section. Since the counter appeared stable with a counting rate of 500kHz (on 1mm²) a lifetime test was attempted at this value. However the detector sparked after 7.5 hours running so the rate was reduced to about 115kHz and a new spot selected. Figure 7 shows the gain measured on this spot as a function of the accumulated charge per cm of anode (20mC/cm was achieved in 468 hours running). The initial rise in the gain with application of the rate is seen; but thereafter the gain is remarkably constant (the effects of changes in the ambient variables have been corrected as described in reference [5]). The small jogs in the curve are usually attributable to the effects of the plate recovering from a rest period.

Scanning across the target spot with a low intensity sample beam reveals a more complex picture than figure 7 would suggest. Figure 8 shows a variety of such scans. Immediately

after a session of strong irradiation a scan shows the beam spot as a region of enhanced gain (as expected). If, however, one leaves the plate to rest for a day or two, the beam spot reveals itself as a region of reduced gain with a very wide and distorted pulse height distribution (figure 9b). Even with quite a modest accumulated charge (6.7mC/cm) the pulse height deficit approaches 70%. This state of affairs requires a rest period of the order of a few days to be established and any irradiation tends to reverse the process. Figure 10 shows the results of an attempt to track the deterioration of the beam spot after irradiation. The transient recoveries evident in the plot appear to reflect the rise of the ambient temperature in the course of the working day. Higher temperature liberates more charge within the glass which compensates the bad effect. The process of measuring the gain also triggers the recovery process and makes it difficult to measure.

The recovery process from the condition of low gain is simple to track. As figure 11 shows, the recovery time increases as the charge dose to the spot is increased. With a 3kHz beam the recovery takes about two hours and with a 1kHz beam, approximately three times as long. The pulse height resolution recovers over the same time scale (figure 12). Converting the time axis in these graphs to the cumulative charge delivered to one square mm of surface shows that the total charge required to restore normal operation is approximately constant and around 800nC/mm² independently of the rate of delivery (figure 13). Clearly there should be some minimum rate necessary to maintain normal operation. We have no figure for this but it seems clear that something of the order of several hundred Hz/mm² would be required.

Figure 14 shows that the reduced gain in the rested beam spot follows the characteristic dependence of proportionality to the log of the accumulated charge. Unfortunately the slope is very steep with 30% gain loss for only 1mC/cm.

4. DISCUSSION

The results show that run in the bias configuration described, the D263 GMSD shows stable operation and remarkable rate capabilities (>100kHz/mm² of 2x10⁵ electron pulses). However, detailed study reveals rate dependent gain effects (about +10% at 30kHz/mm²) which show the characteristic time constant of ion movement in the borosilicate substrate. Under heavy irradiation the avalanches affect the substrate in some self-compensating process which ensures that, as long as the avalanches are present, the gain of the counter remains remarkably constant (in our test, out to 20mC/cm). When the counter is rested (only cosmic rays incident) the gain and pulse height resolution deteriorate drastically in the course of a day or two and there is some evidence that ambient temperature plays a part in the precise history of this process. On applying avalanches again to the surface a complete recovery takes place when about 800nC have been delivered to the beam spot. It is not known precisely what minimum rate would be necessary to maintain proper operation of the detector; we estimate that a few hundred Hz/mm² is probably sufficient.

The results of reference [7] show that at very high charge dose rates (>30nA/mm²) the D263 detector shows negligible gain loss up to 40mC/cm, but at lower dose rates (<13nA/mm²) a significant droop of 6-7% is observed. Our tests were carried out at 3.9nA/mm² and so compare best with the low dose data of the CERN workers. It is difficult to conclude that we find any significant gain drop in the standard measurement procedure, though it is almost

certain that the same substrate effects which we observe are responsible for the dose-dependent effects reported in reference [7].

The reversibility of the gain changes and the time constants involved make it clear that substrate instability is indeed responsible for these effects (and not any polymer deposit - we see no such time-dependent effects in quite heavily polymer-coated electronic glass substrates). Such effects would make one naturally hesitate to accept such detectors for long-term operation in the harsh environment of an LHC tracker. However, if the excellent behaviour exhibited by the thin substrate detector operated with a high drift field and a back plane at anode potential could be combined with the stable operation associated with electronic conducting glass, then a promising detector would result. We are pursuing the option of sputtering a thin coating of semiconducting glass on to thin borosilicate glass to see if the benefits of a low radiation length can be obtained simultaneously with the desirable properties of the semiconducting glass substrate.

REFERENCES

1. A Oed, Nucl Instr & Meth A263 (1988) 351-359
2. J E Bateman and J F Connolly, Substrate-induced instability in gas microstrip detectors. RAL-92-085
3. J E Bateman and J F Connolly, The experimental characterisation of gas microstrip detectors I. Gain characteristics RAL-93-090
4. J E Bateman and J F Connolly, The experimental characterisation of gas microstrip detectors II. Counting rate characteristics RAL-93-096
5. J E Bateman, J F Connolly, Yu N Pestov, L I Shekhtman, R Mutikainen and I Suni, The experimental characterisation of gas microstrip detectors III. Lifetime characteristics. RAL-94-114
6. F Angelini et.al., Development of a large area Microstrip Gas Chamber for the CMS central tracking system, INFN-Pisa/AE 94-011, to be published in Nucl Instr & Meth.
7. R Bouclier, M Capeans, C Garabatos, G Manzin, G Million, L Ropelewski, F Sauli, L I Shekhtman, T Temel, G Della Mea, G Maggioni and V Rigato, Development of micro-strip gas chambers for high rate operation, CERN-PPE/95- Presented at the Vienna Wire Chamber Conference, Feb 13-17 1995

FIGURE CAPTIONS

Figure 1.

The behaviour of the gain of the D263 GMSD after the anode-cathode bias is applied.

Figure 2

The gain and pulse height resolution plotted along the active length of the D263 test counter.

Figure 3

The gain and pulse height resolution of the D263 test counter as a function of the drift potential (Cathode potential = -626V).

Figure 4

The gain of the D263 test counter as measured from the pulse height on a cathode ray oscilloscope. The duration of the measurement period was approximately five minutes.

Figure 5

The time evolution of the gain of the D263 test counter when a fresh area of detector is exposed to different count rate densities (measured on a pulse height analyser).

Figure 6

A plot of the asymptotic gain reached by the D263 test counter at different count rate densities.

Figure 7

A plot of the gain of the D263 test counter as a function of the accumulated charge when *continuously* exposed to a current density of $\approx 4\text{nA}/\text{mm}^2$.

Figure 8

A scan of the gain of the D263 test counter across the active area at various stages during the irradiation of a 1mm^2 spot at $X=310\text{mm}$.

Figure 9

- (a) The pristine pulse height spectrum of 8keV xrays.
- (b) The pulse height spectrum after $6.7\text{mC}/\text{cm} + 3.5$ days resting (HT on).
- (c) The pulse height spectrum of (b) after 2.5 hr of $3\text{kHz}/\text{mm}^2$ of xrays.

Figure 10

The deterioration of the gain and pulse height resolution in the beam spot after the removal of the xray flux ($4\text{nA}/\text{mm}^2$).

Figure 11

The recovery of the gain when xray rate is reapplied to a rested (previously irradiated by different amounts) surface.

Figure 12

The recovery of the pulse height resolution when xray rate is reapplied to an irradiated and rested surface.

Figure 13

A plot of the recovery of the gain (after irradiation and resting) with different xray count densities, against the cumulative charge density delivered to the beam spot during the recovery phase.

Figure 14

A plot of the gain in the "resting dip" at the beam spot as a function of the cumulative charge dose delivered to the beam spot.

Figure 1

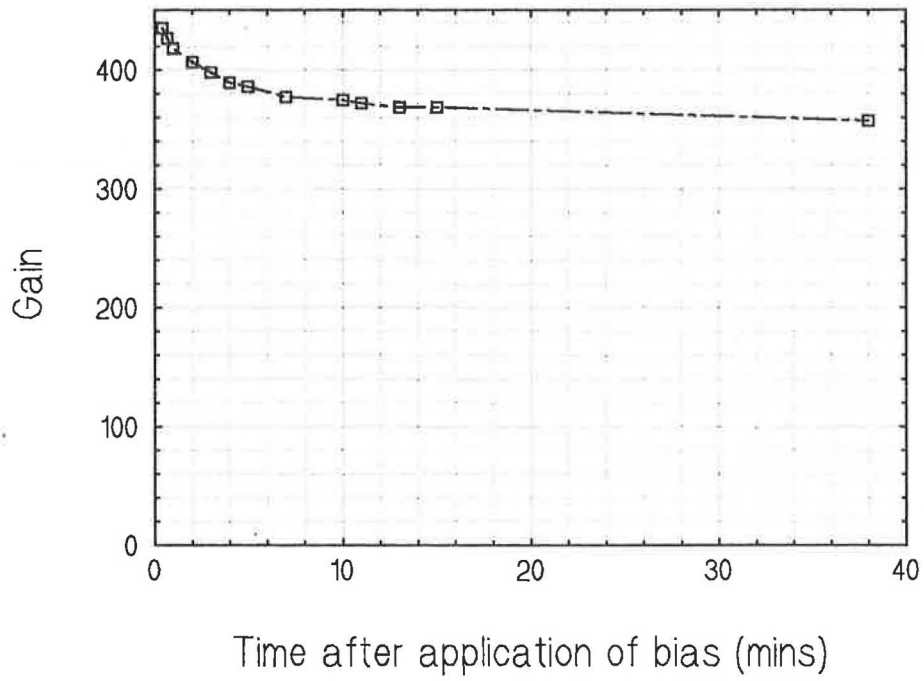


Figure 2

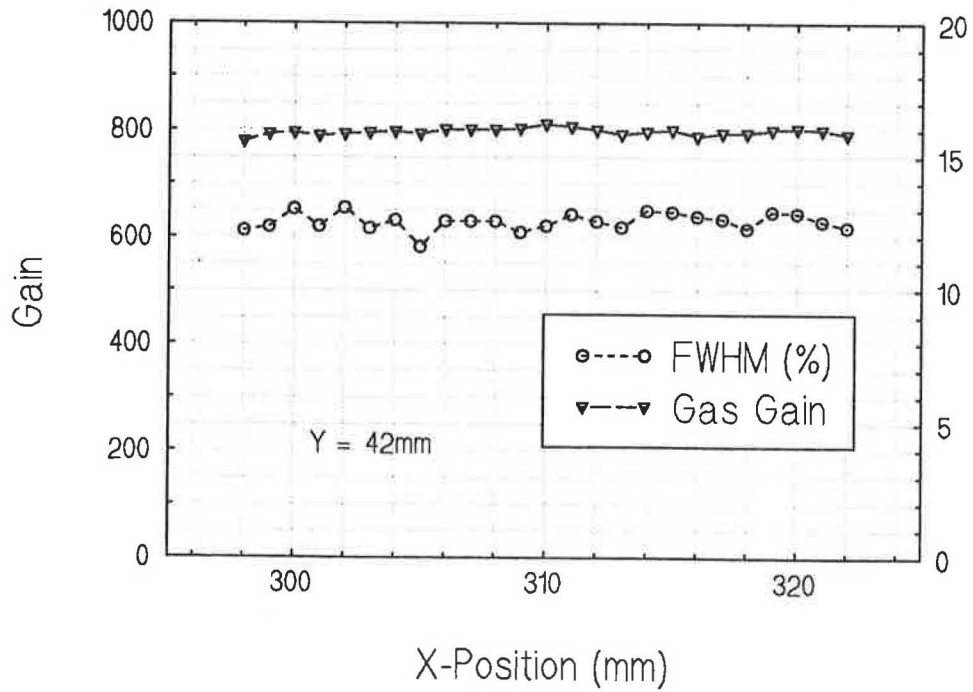


Figure 3

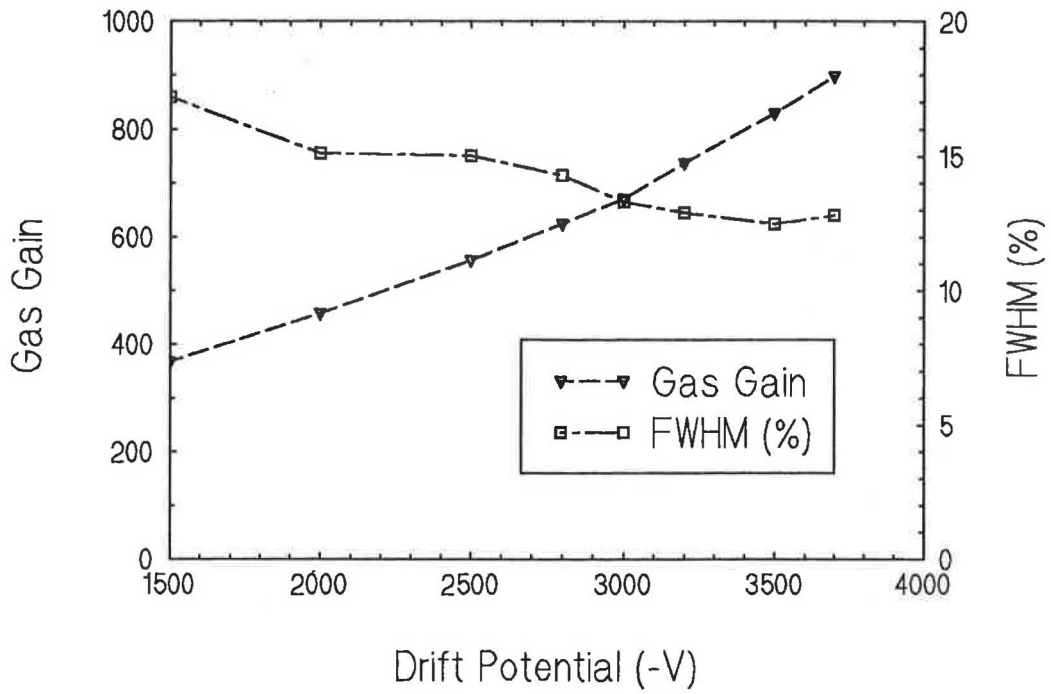


Figure 4

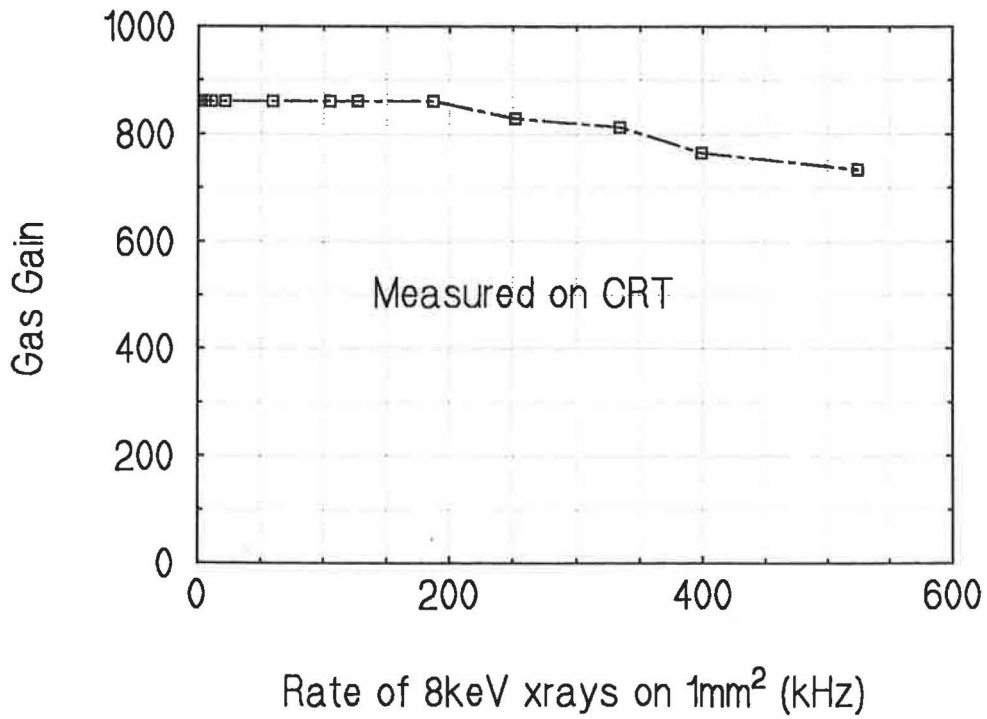


Figure 5

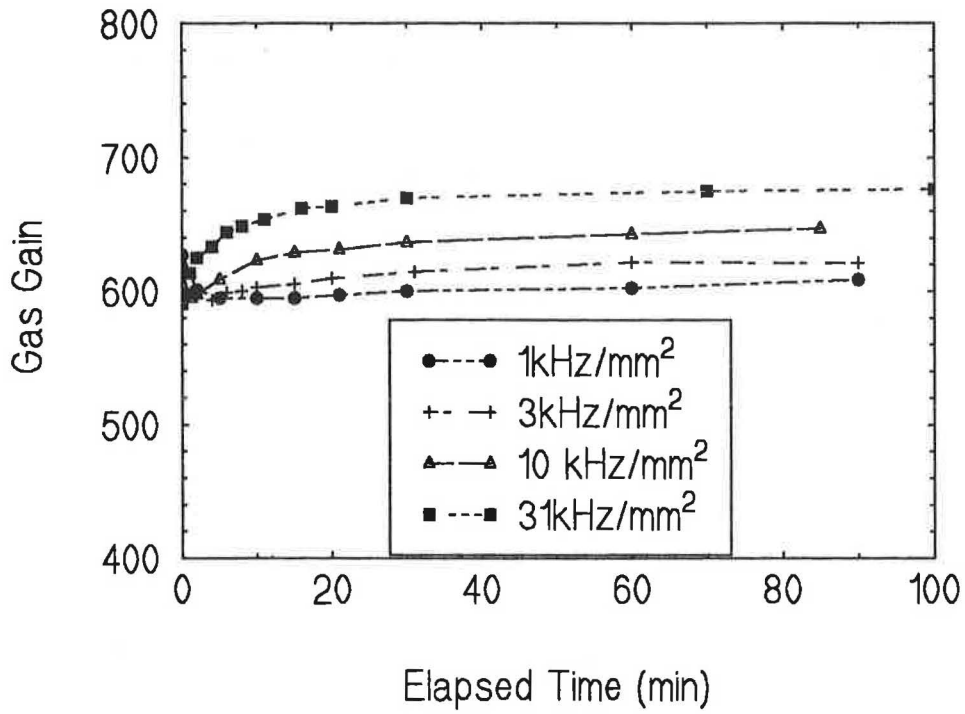


Figure 6

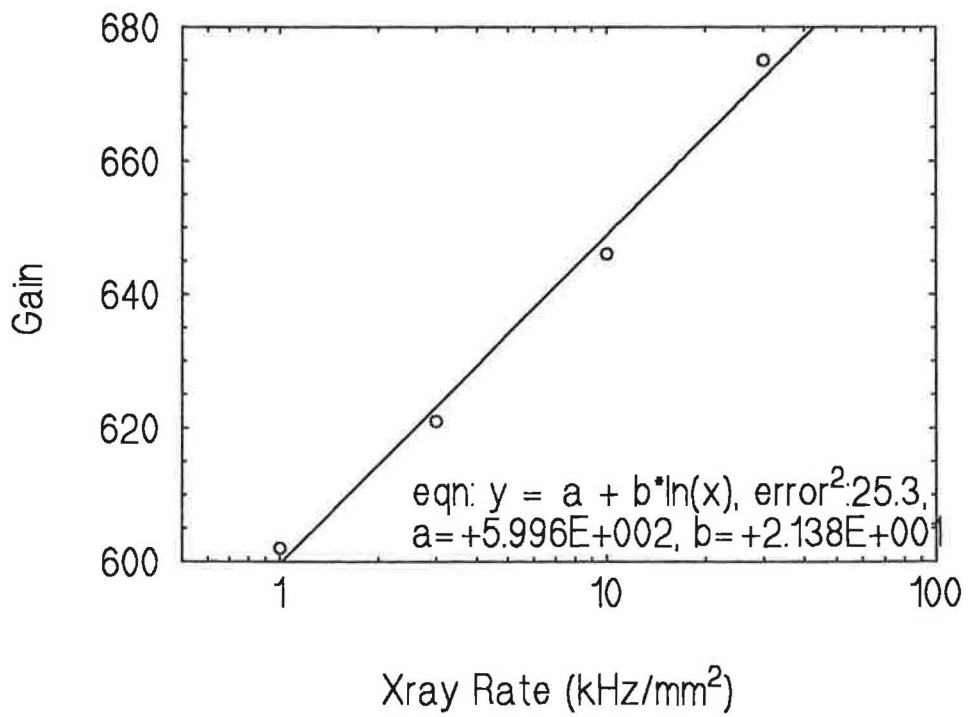


Figure 7

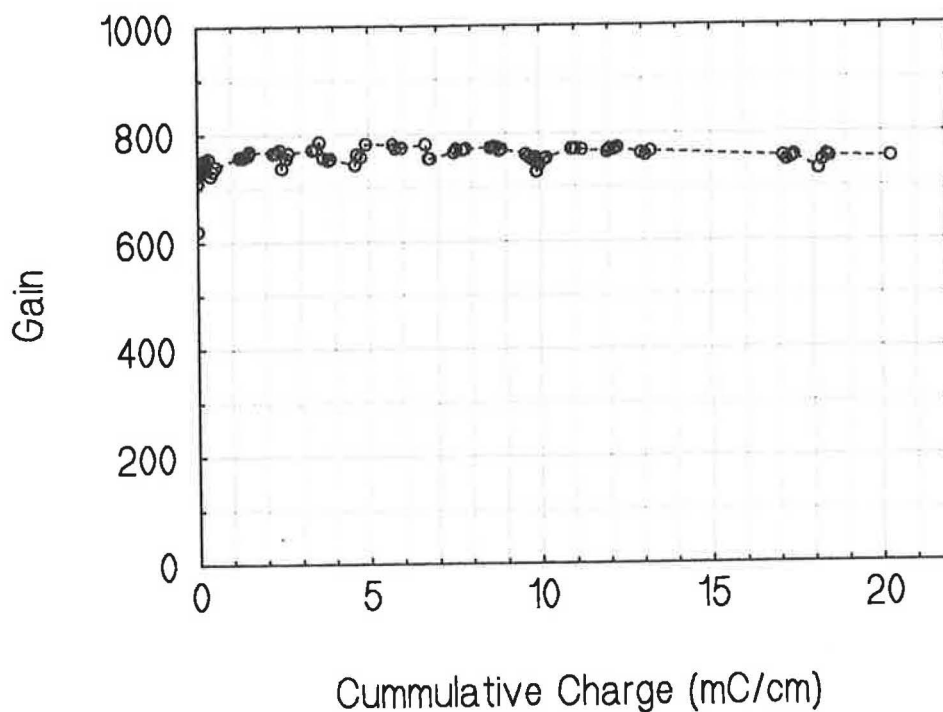


Figure 8

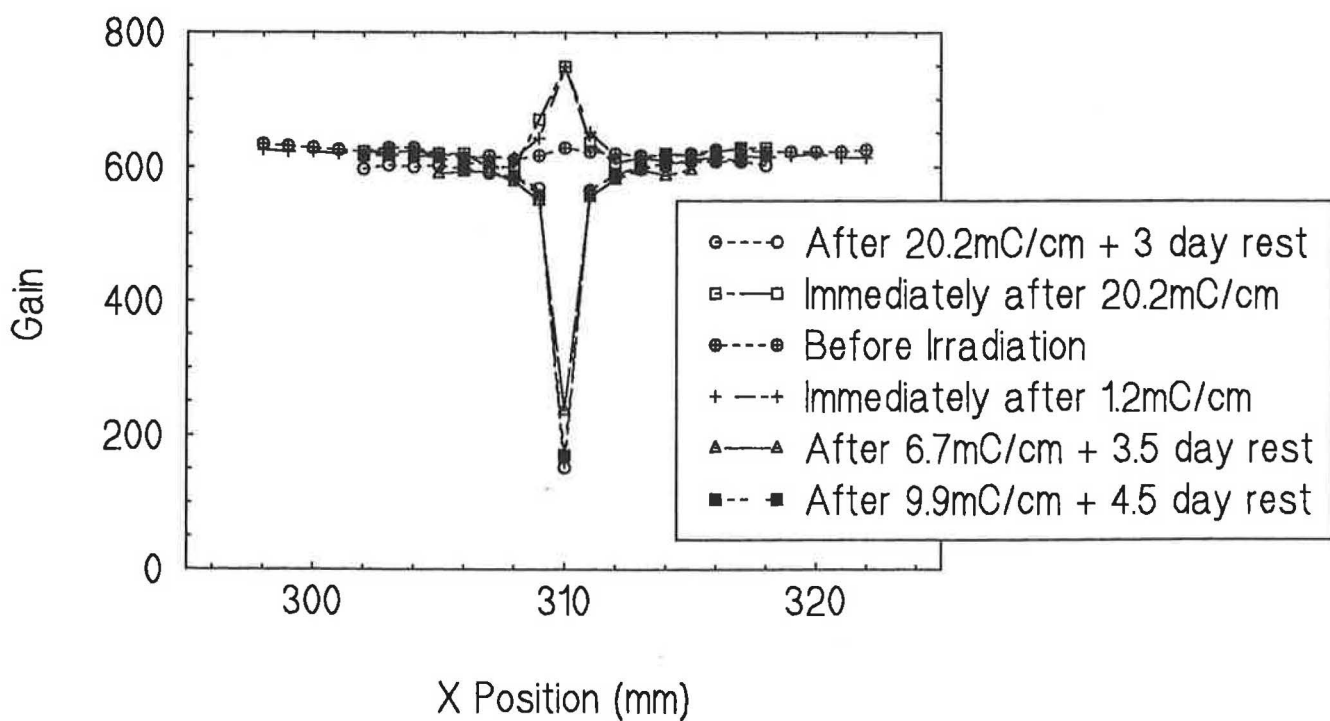


Figure 9

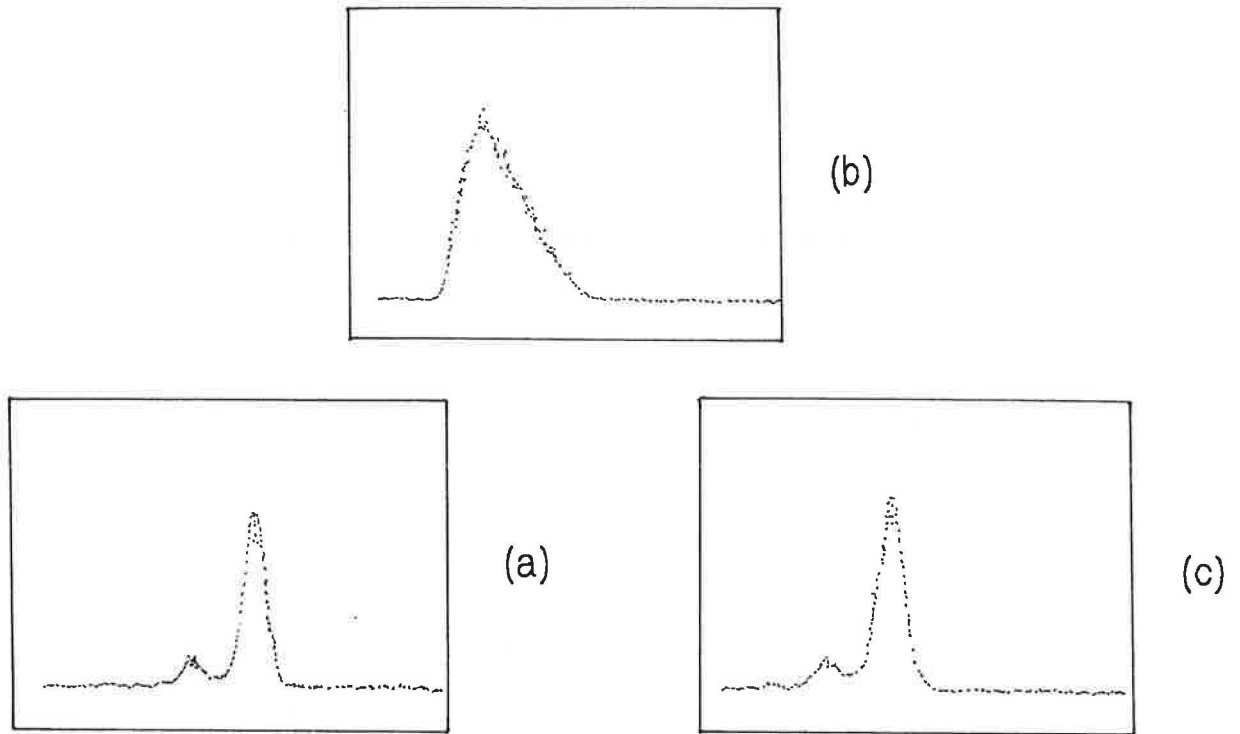


Figure 10

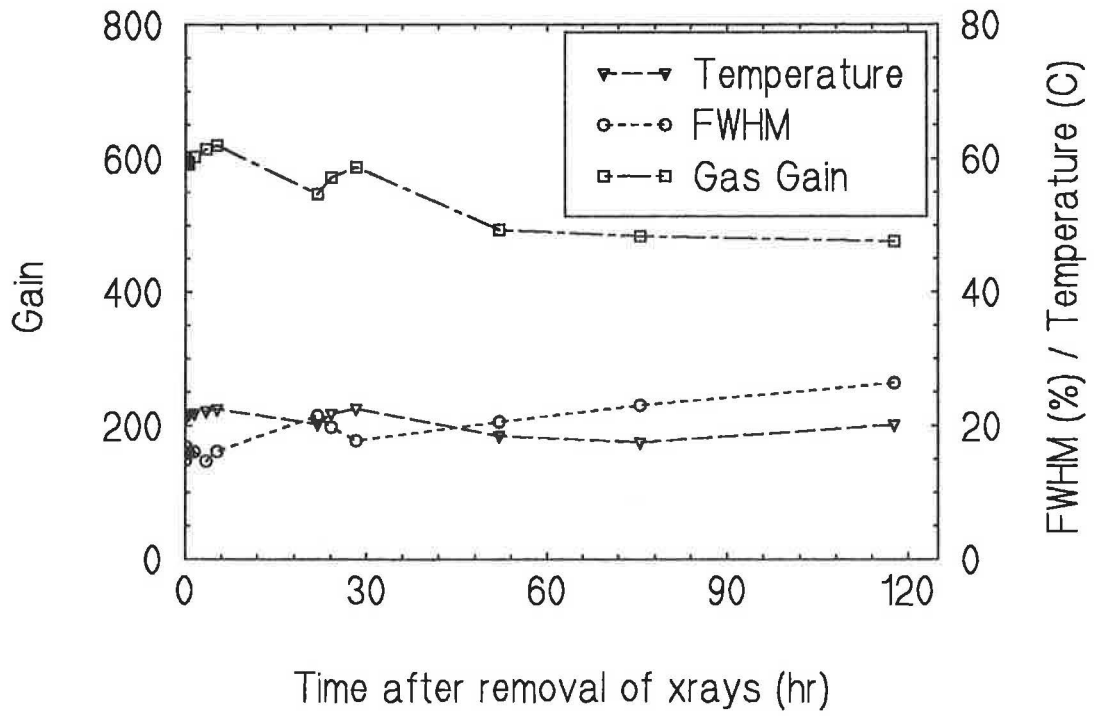


Figure 11

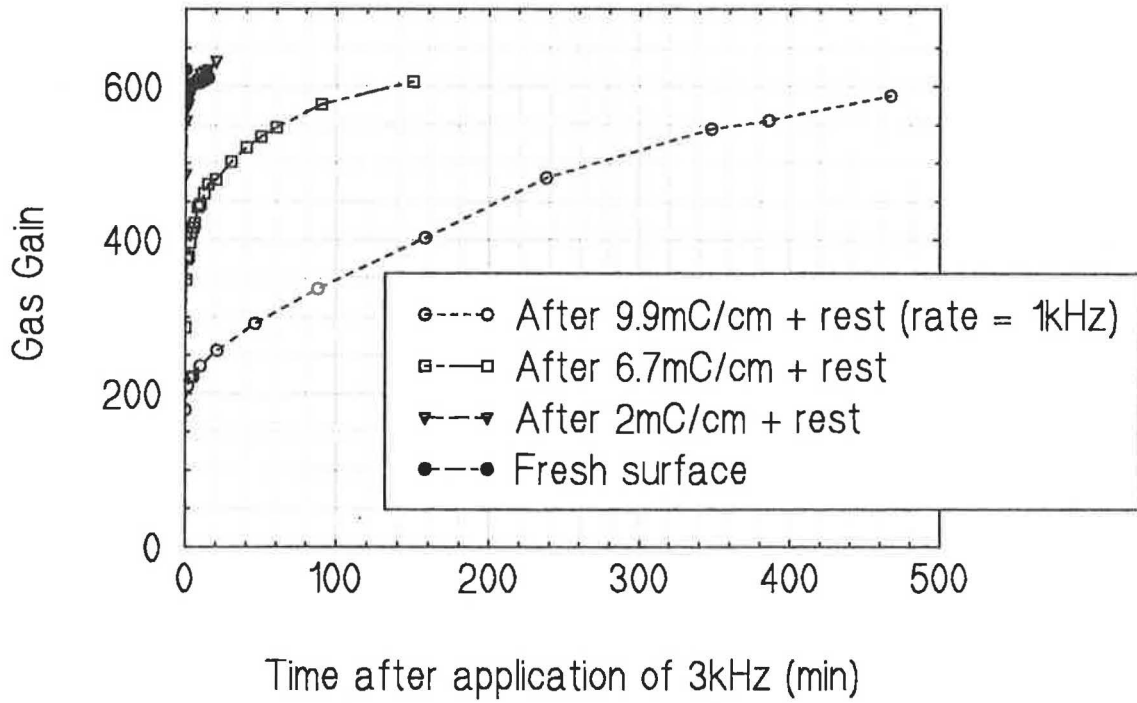


Figure 12

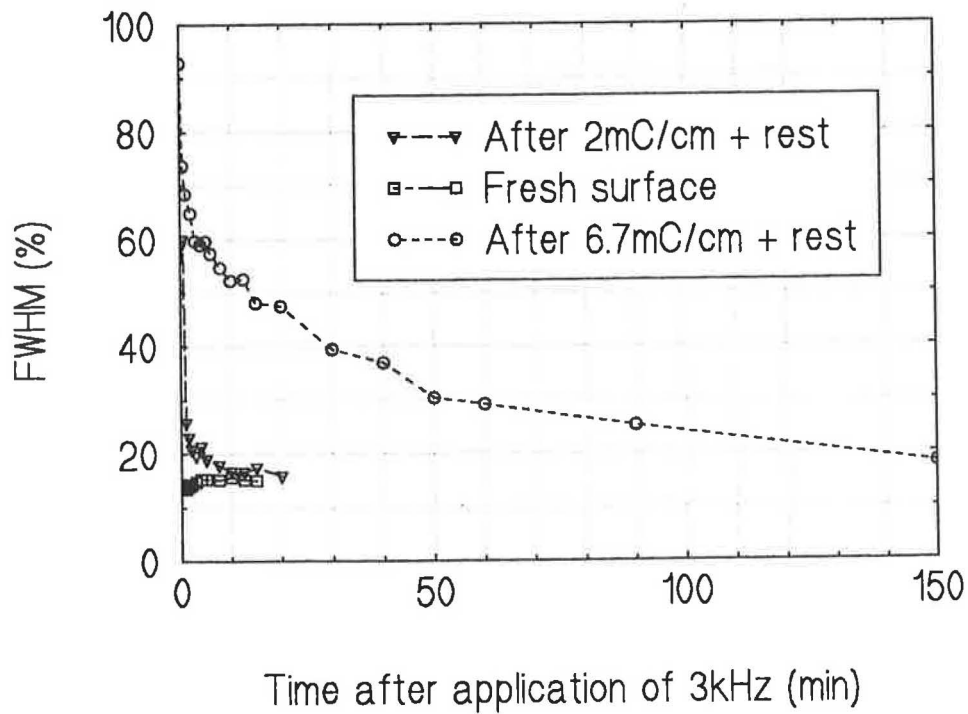


Figure 13

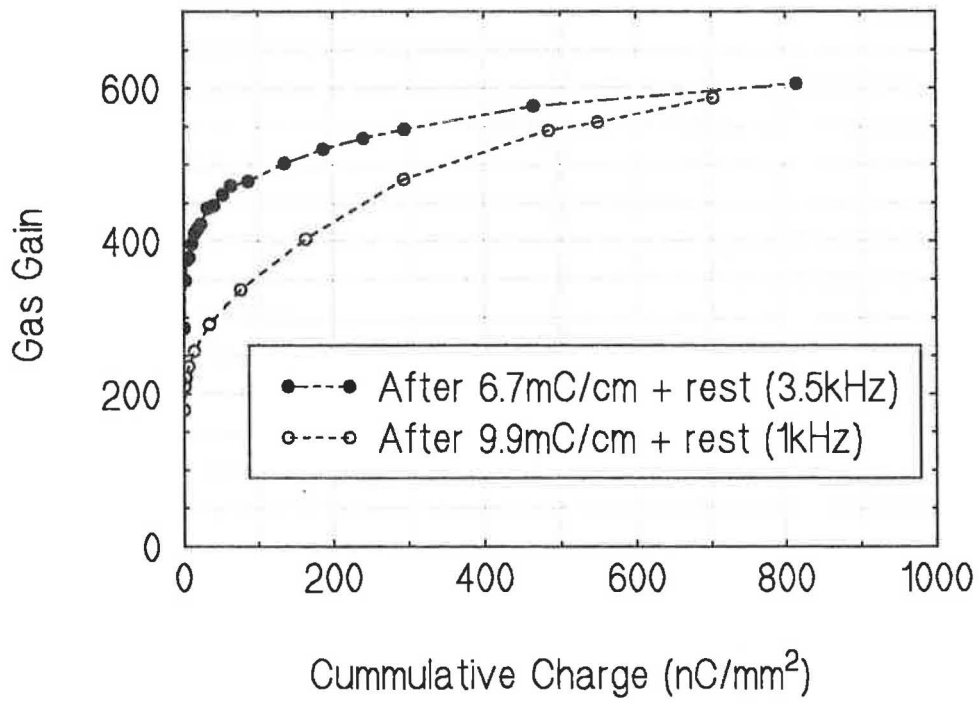


Figure 14

